Contents lists available at ScienceDirect

Psychiatry Research: Neuroimaging

journal homepage: www.elsevier.com/locate/psychresns
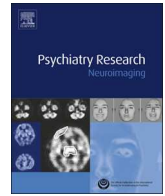
*Neu*³*CA-RT*: A framework for real-time fMRI analysis

Stephan Heunis[a,*], René Besseling[a,b], Rolf Lamerichs[a,c], Anton de Louw[a,b], Marcel Breeuwer[d,e], Bert Aldenkamp[a,b,f,g], Jan Bergmans[a]

[a] *Department of Electrical Engineering, Eindhoven University of Technology, Postal address: PO box 513; Flux buidling, room 7.066, 5600MB Eindhoven, The Netherlands*
[b] *Department of Research and Development, Epilepsy Centre Kempenhaeghe, Heeze, The Netherlands*
[c] *Philips Research Laboratories Eindhoven, Eindhoven, The Netherlands*
[d] *Department of Biomedical Engineering, Eindhoven University of Technology, Eindhoven, The Netherlands*
[e] *Philips Healthcare, Best, The Netherlands*
[f] *Laboratory for Clinical and Experimental Neurophysiology, Neurobiology and Neuropsychology, Ghent University Hospital, Ghent, Belgium*
[g] *Department of Neurology, Maastricht University Medical Center, Maastricht, The Netherlands*

ARTICLE INFO

ABSTRACT

Real-time functional magnetic resonance imaging (rtfMRI) allows visualisation of ongoing brain activity of the subject in the scanner. Denoising algorithms aim to rid acquired data of confounding effects, enhancing the blood oxygenation level-dependent (BOLD) signal. Further image processing and analysis methods, like general linear models (GLM) or multivariate analysis, then present application-specific information to the researcher. These processes are typically applied to regions of interest but, increasingly, rtfMRI techniques extract and classify whole brain functional networks and dynamics as correlates for brain states or behaviour, particularly in neuropsychiatric and neurocognitive disorders. We present *Neu*³*CA-RT*: a Matlab-based rtfMRI analysis framework aiming to advance scientific knowledge on real-time cognitive brain activity and to promote its translation into clinical practice. Design considerations are listed based on reviewing existing rtfMRI approaches. The toolbox integrates established SPM preprocessing routines, real-time GLM mapping of fMRI data to a basis set of spatial brain networks, correlation of activity with 50 behavioural profiles from the BrainMap database, and an intuitive user interface. The toolbox is demonstrated in a task-based experiment where a subject executes visual, auditory and motor tasks inside a scanner. In three out of four experiments, resulting behavioural profiles agreed with the expected brain state.

1. Introduction

Real-time functional magnetic resonance imaging (rtfMRI) involves the online measurement of a subject's neural activity, indirectly, through the measurement of the blood oxygenation level-dependent (BOLD) signal. After preprocessing and analysing these data within the repetition time (TR) the researcher has access to these dynamic results while the subject is inside the scanner. This stands in contrast to conventional fMRI, where image processing is applied after the full set of fMRI scans has been acquired. Since the first published implementation of rtfMRI in 1995 (Cox et al., 1995) the ensuing two decades saw a substantial increase of research interest and activity in this field. Advancements in medical imaging technology (reviewed by Cohen, 2001; Weiskopf et al., 2007), computational algorithms (reviewed by Cohen, 2001; Weiskopf et al., 2007; deCharms, 2007) and computer processing power allow increasingly faster and more advanced acquisition and

processing of functional images and give researchers and clinicians access to data and results in real-time that would otherwise only be available hours, days or weeks after scanning (Weiskopf, 2012).

The application of rtfMRI, initially proposed as a tool to monitor data quality, to easily develop new task and stimulus protocols, and for use in interactive neurological experiments (Cox et al., 1995), has expanded to include: real-time data quality assurance and patient compliance checking (Voyvodic, 1999), pre-experimental or pre-surgical functional localisation and intraoperative guidance (see for example Hirsch et al., 2000; Binder, 2011), neurofeedback studies and treatment (see Weiskopf, 2012; deCharms, 2008; Sulzer et al., 2013; Sitaram et al., 2016, for extensive reviews), and teaching (Weiskopf et al., 2007). Increasingly, applied rtfMRI is viewed as a useful diagnostic and treatment (navigation) tool in psychoradiology, a growing field described as the use of radiologic approaches for diagnosis, treatment planning and monitoring of patients with major neuropsychiatric

---

disorders (Lui et al., 2016).

Apart from the basic real-time processing capabilities integrated into the hardware of all major MRI vendors, several proprietary, custom in-house and open-source rtfMRI solution sets or toolboxes have been developed at various locations worldwide. These include *FIRE* (Gembris et al., 2000) and *TurboFIRE* (Gao and Posse, 2003), *scanSTAT* (Cohen, 2001), AFNI's real-time plugin (https://afni.nimh.nih.gov/; Cox, 1996), *Turbo-BrainVoyager* (Brain Innovation, Maastricht, the Netherlands; Goebel, 2012), *STAR* (Magland et al., 2011), *FRIEND* (Sato et al., 2013), the *FieldTrip* toolbox's rtfMRI extension (http://www.fieldtriptoolbox.org/development/realtime/fmri; Oostenveld et al., 2011), *BART* (Hellrung et al., 2015) and more recently *OpenNFT* (Koush et al., 2017). While these toolboxes allow a wide range of rtfMRI processing and neurofeedback signal calculation capabilities, most clinical studies reporting the use of rtfMRI (in particular most neurofeedback studies) have focused on analysing, visualising and feeding back activation changes for particular ROIs in the brain that are associated with the disorder or condition being studied (see for example Alegria et al., 2017; Young et al., 2017; Ruiz et al., 2013; Subramanian et al., 2011; Nicholson et al., 2017). In most neuropsychiatric conditions, however, an array of complex brain functions such as cognition are affected, processes that are increasingly regarded as being mediated by synchronous activity across multiple brain regions (Mišić and Sporns, 2016). To improve learning effects in neurofeedback training experiments conducted in subjects with these conditions, the operant conditioning model requires feedback to be contingent on the brain mechanism believed to underlie the condition (Weiskopf et al., 2004). Thus, it is hypothesized that a feedback signal calculated based on a model that reflects a richer understanding of the underlying neural mechanism could be an improved approach over ROI-based methods in cases where complex brain function is involved. To enable further development and testing of this hypothesis, rtfMRI toolsets and neurofeedback studies should expand to include a particular focus on the analysis of dynamic and spatially distributed brain activity, in addition to ROI-based approaches.

The dynamics and spatial distribution of functional brain networks at rest have been widely investigated and reported. Resting state networks tend to show separable spatial patterns with distinct temporal characteristics during rest- or task-based experimental paradigms (Beckmann et al., 2005). Differences in resting state network characteristics between subjects with neuropsychiatric disorders and healthy subjects have also been studied and used as the basis for potential biomarkers (see e.g. Whitfield-Gabrieli and Ford, 2012, for a review focusing on the default mode network). Recently, Karahanoğlu and Van de Ville (2015) applied temporal deconvolution and clustering techniques to resting state fMRI time series to yield spatially and temporally overlapping co-activation patterns. These iCAPs form dynamically assembling building-blocks for resting state networks, and each pattern has been associated with a consistent behavioural profile using the Brainmap database (http://www.brainmap.org/; Laird et al., 2005). These aspects, that is the spatially distributed and dynamic nature of the iCAPs patterns as well as their relation to behavioural brain state interpretations, suggest that they could be useful as targets for neurofeedback calculation in rtfMRI neurofeedback experiments relating to neuropsychiatric conditions.

In this article we introduce *Neu³CA-RT*, a Matlab-based framework for rtfMRI analysis developed at the Neu³CA research group (http://neu3ca.org/background/neu3ca/) at the Eindhoven University of Technology. Based on design considerations obtained from reviewing previous and current state of the art rtfMRI solutions and methodologies, we describe the experimental setup and image (pre)processing steps central to the framework. We present an exploratory rtfMRI analysis implementation, which is based on a dynamic spatial general linear model (GLM) fit of Karahanoğlu and Van de Ville's innovation-driven coactivation patterns (iCAPs) (Karahanoğlu and Van de Ville, 2015) to real-time fMRI data and the subsequent mapping to behavioural brain states. The method is demonstrated by subjecting a healthy control to several known behavioural paradigms and comparing the data-driven network analysis and behavioural interpretation to the expected brain state(s). We conclude by discussing the results and future work.

1.1. Design considerations for a rtfMRI toolbox

Several aspects of existing rtfMRI toolsets influence their performance and area of application. These include the particular technical infrastructure and imaging parameters, pre-real-time processing, preprocessing, image analysis, program execution time and software design. When assessing the performance of real-time toolsets, specific attention should be given to latency, i.e. the total delay of the real-time processing chain between image acquisition and availability of the analysis results, and the achievable throughput, i.e. the quantified output per time period (in our case, analysed images per second or, similarly, TR).

Particulars of how rtfMRI aspects have been implemented in existing toolsets, especially artefact correction and ROI and whole-brain processing algorithms, have been reviewed extensively elsewhere (Weiskopf et al., 2007; LaConte, 2011; Caria et al., 2012). For the purpose of this article, important design considerations (and, where applicable, their influence on latency and throughput) are described below.

1.1.1. rtfMRI technical setup

The specifics of the MRI scanner, processing hardware and the accompanying rtfMRI software package are considered. In principle, rtfMRI should be achievable with any modern MRI scanner that has online image reconstruction and network communication capabilities, although custom development is typically necessary to facilitate transporting or sharing image data between scanner hardware and the device used for real-time processing, whether this is the scanner console or a network location. Dedicated development has also been done to integrate rtfMRI processing directly into scanner hardware 1995 (Cox et al., 1995, Cohen, 2001, LaConte et al., 2007). Ideally, all major MRI vendor hardware should be able to export acquired images in real-time to a network location, from which the preferably vendor-agnostic rtfMRI software package would then collect and process the data. Both the *Turbo-BrainVoyager* and *OpenNFT* toolboxes employ such a server-client setup and are compatible with scanners from multiple MRI vendors. *Neu³CA-RT* has been implemented similarly, facilitated by real-time data transfer software developed in collaboration with Philips.

The technical setup extends from the scanner to external hardware and software. Firstly, rtfMRI packages need to be easily understood and easily adaptable to facilitate widespread use. As reported by Koush et al. (2017), interpreted languages like Matlab (MathWorks, Natick, Massachusetts, United States) and Python (https://www.python.org/) allow intuitive understanding and easier sharing of code and continued collaborative tool development by a wide-ranging and large user base. This is strengthened further by the existence of SPM (www.fil.ion.ucl.ac.uk/spm), FSL (https://fsl.fmrib.ox.ac.uk/fsl) and AFNI (https://afni.nimh.nih.gov/), three of the most widely used platform-independent and freely available fMRI analysis libraries that can readily be incorporated into interpreted language programs. When optimising for widespread use and whenever possible, rtfMRI toolboxes should exploit these libraries and frameworks. While acknowledging that commercial tools like Matlab provide barriers to unconditional dissemination of software tools and knowledge, our familiarity with the programming environment and its widespread use in research and educational institutions led to the initial version of *Neu³CA-RT* being based in Matlab and using SPM12.

Secondly, the central or graphical processing unit (CPU or GPU) of a designated image processing computer needs to have enough power so as to minimise real-time latency while managing a tradeoff between

processing speed and all factors restricting increased processing power (these might include cost, logistical impediments and site-specific restrictions). To facilitate ease of implementation, a personal computer (PC) with 16GB RAM and a 4-core GHz-range processor is recommended for a rtfMRI setup like *Neu³CA-RT*. Increased processing power could be warranted if the resulting latency is too high for the desired throughput, while more complicated pipelining and parallelization of real-time processes could be considered (either at application-level, computationally on a single PC or at hardware level on multiple machines) if throughput needs to be increased.

1.1.2. rtfMRI image quality considerations

Echo-planar imaging (EPI) is widely used in fMRI imaging sequences and provides a sound, although not exclusive, basis for rtfMRI. The use of multi-echo imaging sequences in real-time (Posse et al., 1999; Weiskopf et al., 2005) has been reported to remove image distortion artefacts and increase BOLD contrast sensitivity through weighted combination of multi-echo images. More recently, Kundu et al. (2012, 2013, 2017) implemented an independent component analysis algorithm (ME-ICA) on full multi-echo EPI datasets to yield significant gains in BOLD CNR. Importantly, imaging parameters like the field-of-view (FOV), voxel resolution, voxel matrix size, repetition time (TR) and echo time (TE) have to be refined so as to manage the tradeoff between increased spatial resolution, increased BOLD sensitivity, and shortened TR, while keeping the specific application in mind. Increased spatial resolution is beneficial when requiring rtfMRI output that is highly spatially localised, but this in turn requires more acquisition and processing time and thus increases latency. Similarly, a short TR (in reviewed literature, typically in the order of 2 s for ROI-based acquisition and real-time processing) is beneficial for more frequent real-time data visibility and neurofeedback, but simultaneously compromises spatial resolution and constrains the amount of available dynamic calculation time, essentially requiring the real-time latency to be less than 2 s if the throughput is to be one analysed image per TR and no pipelining is used.

Selection of a short TR is further motivated by the need to identify distributed changes in BOLD signal response (from a predefined baseline) as soon as they occur. In a task paradigm the general haemodynamic response function characteristics are well established: an initial post-stimulus delay of 1–2 s and a peak at 4–6 s, reaching a plateau if the stimulus is sustained (Bandettini et al., 1992). For a controlled task time course with an expected response, less incentive exists for shortening the TR, but for the comparatively unknown dynamics of resting state fMRI data this is not the case. Here, more frequent sampling enables a real-time description of dynamic data, which is especially useful if this description needs to be acted on in real-time.

Real-time denoising or preprocessing is required to provide further image quality improvements. Previously implemented algorithms include those for image distortion correction, prospective or retrospective 3D motion correction, temporal filtering and spatial smoothing (reviewed by Weiskopf et al., 2007). Prospective motion correction typically incorporates real-time data from optical motion tracking systems, such as described by Zaitsev et al. (2006), or is implemented to estimate and apply a 3D transformation during reconstruction of each EPI image. Other confounders of real-time BOLD activation are artefacts resulting from subject physiology like heartbeat and respiration, as well as EPI artefacts resulting from gradient coil heating and other scanner instability effects. Technical setup allowing, physiological data should be sent dynamically to the applicable rtfMRI toolbox for continuous monitoring (for example Voyvodic, 1999) and correction (for example Smyser et al., 2001).

In general, any imaging parameters or preprocessing approaches such as those described above that fundamentally improve the signal-to-noise-ratio (SNR) are important to improve spatiotemporal resolution and hence to reduce latency for a specified spatial resolution. However such approaches should themselves have limited latency to

ensure that there is a net improvement in overall latency.

With the aim of acquiring and describing distributed BOLD activity in specific (sub)networks of the brain, the imaging parameters for current *Neu³CA-RT* experiments were selected to favour increased spatial resolution (1.75 × 1.75 × 3 mm per voxel, see *Data Acquisition* in the *Materials and Methods* section) over a short TR, resulting in a TR of 3 s which can be considered standard in a task-based paradigm.

1.1.3. rtfMRI image analysis considerations

Reviewed literature shows a wide variety of mass univariate and multivariate analysis algorithms being implemented in rtfMRI. Historically, statistical methods like t-tests, correlation analysis (Voyvodic, 1999), GLMs and multiple regression (for example Bagarinao et al., 2003) formed the basis of analysing single ROI activation or identifying artefacts in real-time. Thus researchers and clinicians are able to view, for example, real-time ROI activation maps or real-time subject motion estimations.

In clinical applications, multiple rtfMRI studies have reported benefits of specific ROI-based neurofeedback as a treatment option in neurological and psychiatric conditions, such as ADHD, depression, schizophrenia, Parkinson's disease and PTSD (see Sitaram et al., 2016, for a review). For studying cognition-related aspects related to whole-brain networks, however, the methodological focus should include analysing spatially distributed and temporally dynamic brain activity. Accordingly, an increasing amount of rtfMRI algorithms using functional connectivity and multivariate pattern analysis (MVPA, also referred to as multi-voxel pattern analysis) have been published and made available in rtfMRI toolsets, including: windowed correlation (Zilverstrand et al., 2014); dynamic causal modelling (Koush et al., 2013); spatial GLMs; independent component analysis (ICA) (Esposito et al., 2003); support vector machines (SVMs) (LaConte et al., 2007); and neural networks (reviewed by LaConte, 2011). Reviewed literature shows that, in the case of machine learning algorithms, the focus is increasingly on quantifying intuitive and interpretable brain states through classification, as opposed to quantifying the lower-level BOLD activation level of specific ROIs and using that for biomarker development or neurofeedback.

In the current version of our *Neu³CA-RT* framework, we implemented an exploratory functional network-based fMRI analysis pipeline that aims to quantify the real-time brain state of the subject by mapping dynamic and spatially distributed brain activity onto known co-activation patterns that relate to certain behavioural profiles. In a recent study, Karahanoğlu and Van de Ville (2015) developed the iCAP model of functional brain networks, which is based on a spatio-temporal regularisation of resting state fMRI data from healthy volunteers. It decomposes fMRI data into a set of 13 generic co-activation patterns (see Fig. 2 of Karahanoğlu and Van de Ville, 2015) that can be used as spatially and temporally minimally overlapping building blocks to describe a variety of dynamic brain network states. These iCAPs have in turn been associated with the set of 50 behavioural domains as defined by the Brainmap database (http://www.brainmap.org/; Laird et al., 2005), a vast online repository of activation maps from fMRI studies (in the order of 3000 papers, 70000 subjects, 15000 experiments and 122000 reported brain locations). This allows for the interpretation of observed networks in terms of constituents of interpretable behavioural categories Action, Cognition, Emotion, Introception and Perception (see Fig. 6 of Karahanoğlu and Van de Ville, 2015). The implementation in the current version of our *Neu³CA-RT* framework thus allows for a real-time (every 3 s) mapping of dynamic whole-brain activity to the 13 innovation-driven co-activation patterns through a spatial GLM (i.e. calculating how well the dynamic brain activity pattern can be explained by known "building block" patterns) and the subsequent association to behavioural profiles through correlation (i.e. how the subject's dynamic brain activity pattern, as explained by the iCAP networks, relates to known behavioural states. This analysis adds real-time throughput steps of voxel masking, executing two GLM

calculations, and calculating correlation coefficients to the *Neu³CA-RT* pipeline. These steps add minimal latency to the real-time process, in the order of 0.3 s (see *Results* section).

In exploring the use of whole-brain activity patterns in real-time, we aim to provide a framework that allows the rtfMRI neurofeedback signal to be calculated from a more representative data sample, which could lead to improved neurofeedback learning effects. Additionally, the access to real-time brain state interpretations in terms of behavioural profiles allows a more intuitive look at dynamically changing brain activity.

1.1.4. rtfMRI program execution considerations

The statement by Cox et al. (1995) that dynamically increasing calculation time in rtfMRI applications is unacceptable remains valid, although improvements in computer processing power can be a mitigating factor. Where possible, new rtfMRI developments should aim to avoid cumulative algorithms (processing larger amounts of data for every iteration) that could lead to problematic increases in calculation time, while taking experiment-specific constraints in terms of TR and number of acquired volumes into account. This applies to all preprocessing and image analysis steps applied to fMRI data during the course of a single TR. Sliding-window approaches (Gembris et al., 2000), recursive algorithms (Cox et al., 1995) and approximations can be implemented to contain the required calculation time.

To minimise real-time program latency, a rtfMRI processing pipeline can be constructed such that real-time processing occurs in the native functional stereotactic space. This removes the real-time preprocessing step of normalisation to a standard space, but necessitates the pre-real-time mapping of standard space model components (if applicable) to the native functional space. This might add time (to the order of 10–20 min) to the overall experiment, but could easily be incorporated into the functional localizer pipeline that is part of a typical neurofeedback experiment. It was thus selected as the desired method for *Neu³CA-RT*.

Furthermore, standard software programming best practices should be implemented to ensure efficient code execution (for example, in Matlab, vectorisation and preallocation of memory). Ultimately, if the desired throughput is to be 1 analysed image per TR, all real-time preprocessing and image analysis steps should result in a total dynamic calculation time less than the selected TR, and with an increasing need to shorten the TR for resting state real-time applications, future rtfMRI toolbox developments should optimise algorithms for speed.

2. Methods

2.1. Experimental setup

Neu³CA-RT was developed and tested using a Philips Achieva MRI scanner (3T) interfaced with an external PC (16GB RAM, 3.2 GHz single core processor) running Windows 7 and Matlab. The program retrieves data from a user-specified location on the processing PC, which could in principle be served by NIfTI data (https://nifti.nimh.nih.gov/) from any network-enabled MRI scanner (provided the ability for real-time fMRI data transfer and conversion to NIfTI format), thus allowing implementations with other MRI vendors. The experimental setup is shown in Fig. 1.

2.2. Data Acquisition

As a preliminary step to real-time image acquisition and processing, both an anatomical and a functional image are acquired. These images are used in the pre-real-time processing steps described below. Anatomical data are recorded using a three dimensional T1-weighted gradient echo sequence (T1 TFE) with scanning parameters: TR = 8.2 ms, TE = 3.75 ms, flip angle 8°, FOV 240 × 240 × 180 mm, resolution $1 \times 1 \times 1$ mm³, total scan time = 6:02 min.

Functional whole brain data are recorded using a gradient echo EPI sequence with scanning parameters: TR = 3000 ms; TE = 30 ms; 45 transverse slices with a slice thickness of 3 mm (no gap); in plane resolution = 1.75 × 1.75 mm; voxel matrix size 128 × 128 × 45; flip angle = 90°; total scan time = 8 min.

2.3. Data transfer

An integral part of the technical rtfMRI setup is having access to functional scans for processing as soon as they are acquired. This is achieved by real-time TCP/IP data transfer from the MRI scanner to an external processing PC through the Philips scanner's *eXTernal Control* (XTC) interface and the *XTC-datadumper* application installed on the processing PC (Smink et al., 2011). These packages were implemented with support from the vendor. The XTC interface allows reconstructed image data to be retrieved from the scanner, which the *XTC-datadumper* then receives and converts to Philips PAR/REC files (one pair per functional image) before storing it in a pre-specified location on the processing PC, ready for import by the rtfMRI toolbox.
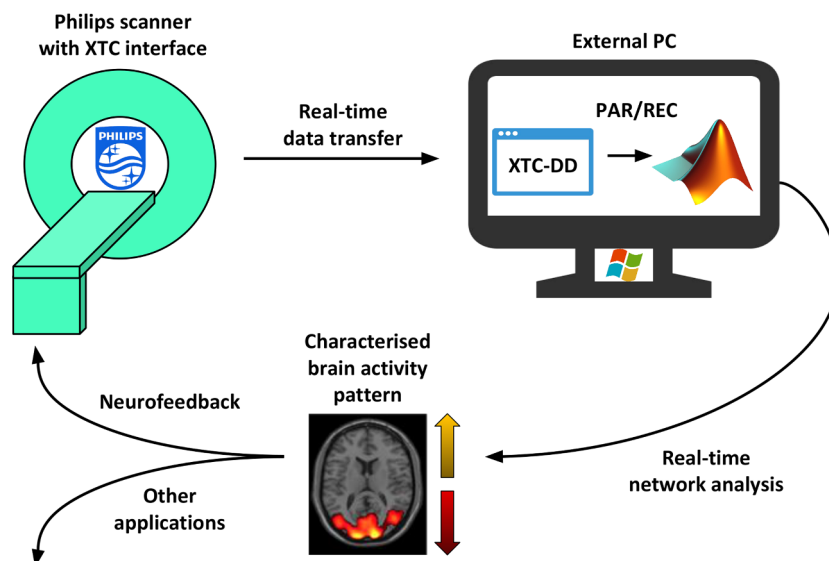

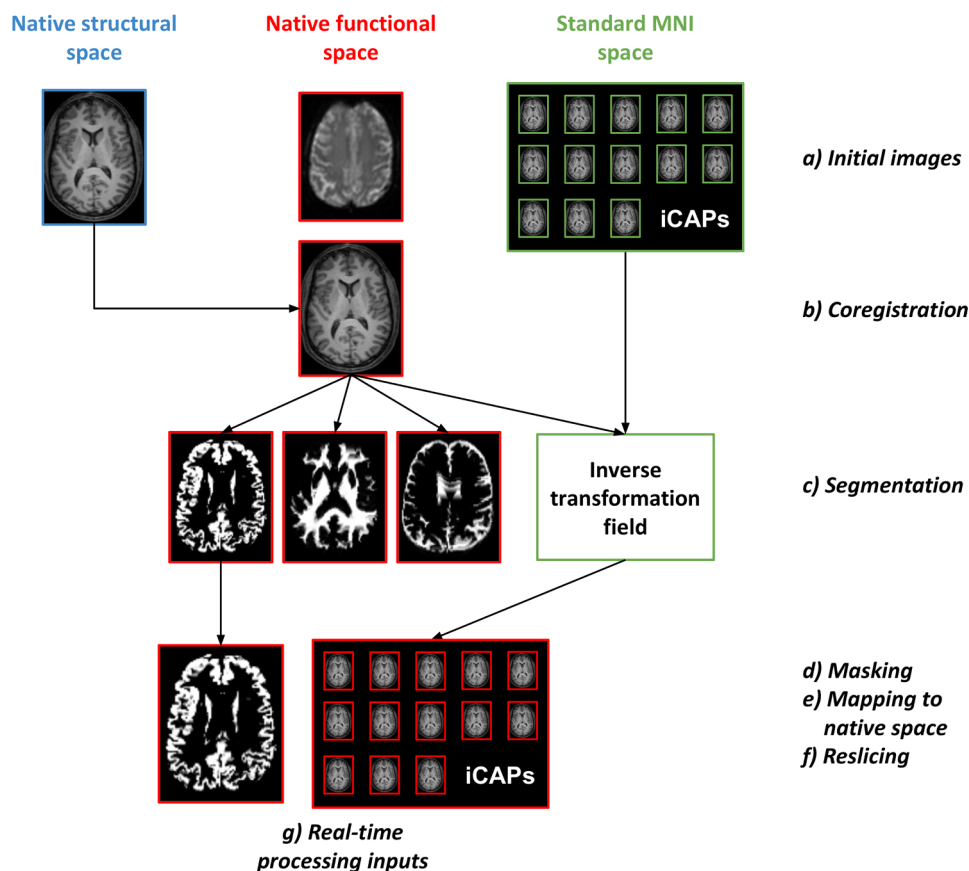**Fig. 1.** The experimental setup of *Neu³CA-RT*

Fig. 2. The pre-real-time processing pipeline.

2.4. Image Processing

All image processing is done in Matlab using a combination of adapted SPM12 routines and self-developed scripts. The pre-real-time and real-time processing pipelines are illustrated in Figs. 2 and 3 and explained below.

2.4.1. Pre-real-time processing

To minimise real-time program execution time, the full pipeline is constructed such that real-time processing occurs in the native functional stereotactic space. Prior to real-time processing, the initial structural image is coregistered to the initial functional image using SPM12′s coregister functionality. The coregistered structural image is then segmented into grey matter, white matter and cerebrospinal fluid (CSF) tissue classes using SPM12′s unified segmentation procedure. This segmentation process also implicitly normalises the coregistered structural image to the standard MNI space (Montreal Neurological Institute; Collins et al., 1994), generating forward and inverse transformations. The inverse transformation is subsequently applied to the 13 iCAPs networks/images to transform them from MNI to the native functional space. Finally, the tissue probability maps and native-space iCAPs images are all resliced to the native functional space grid, thus allowing for direct comparison of voxels.

2.4.2. Real-time processing

For every functional dynamic (i.e. once every TR), the *XTC-data-dumper* sends a PAR/REC file pair to a prespecified location on the external PC. These files are converted to NIfTI format (https://nifti.nimh.nih.gov/) using a modified version of *r2agui* (http://r2agui.sourceforge.net/). Once converted, the dynamic functional NIfTI

image is realigned to the first functional image (which can be user-specified as the initial pre-real-time functional image, or the first image in the real-time series) using a least squares approach and a 6 parameter rigid body transformation. The algorithms for the motion correction steps were adapted from the "spm_realign_rt" and "spm_reslice_rt" routines of the OpenNFT codebase (https://github.com/OpenNFT/OpenNFT), which were originally adapted from SPM12 to minimize execution time. A binary mask derived from the grey matter tissue class image is then applied to the realigned functional image. From this point onward, standard matrix calculations are done from in Matlab on matrix data retrieved from each dynamic NIfTI image.

To determine how the iCAPs model of network-building-blocks fits the dynamic fMRI data, a spatial GLM containing the iCAPs spatial maps is subsequently applied, with the 13 most frequently occurring iCAP images (as the desired model) and the mean functional image (derived from the full 4D fMRI dataset) as the spatial design matrix regressors. As the model aims to describe spatial activity differences in terms of distinct co-activation patterns, the image mean is included so as to describe the majority of the observed signal in the dynamic functional image. This allows the 13 iCAP regressors to describe any additional up- or down-regulated activity across grey matter. Beta values resulting from the spatial GLM are corrected for drift and for realignment residuals by applying a temporal GLM with the 6 realignment movement parameters and linear and quadratic drift terms as regressors.

The GLM steps generate a list of iCAP network weights (beta values) that indicate in which relative proportion the iCAP network building blocks best describe the current fMRI activity with respect to the image mean. To convert these weights into interpretable information, they are correlated (using Pearson's linear correlation) with the 50 behavioural
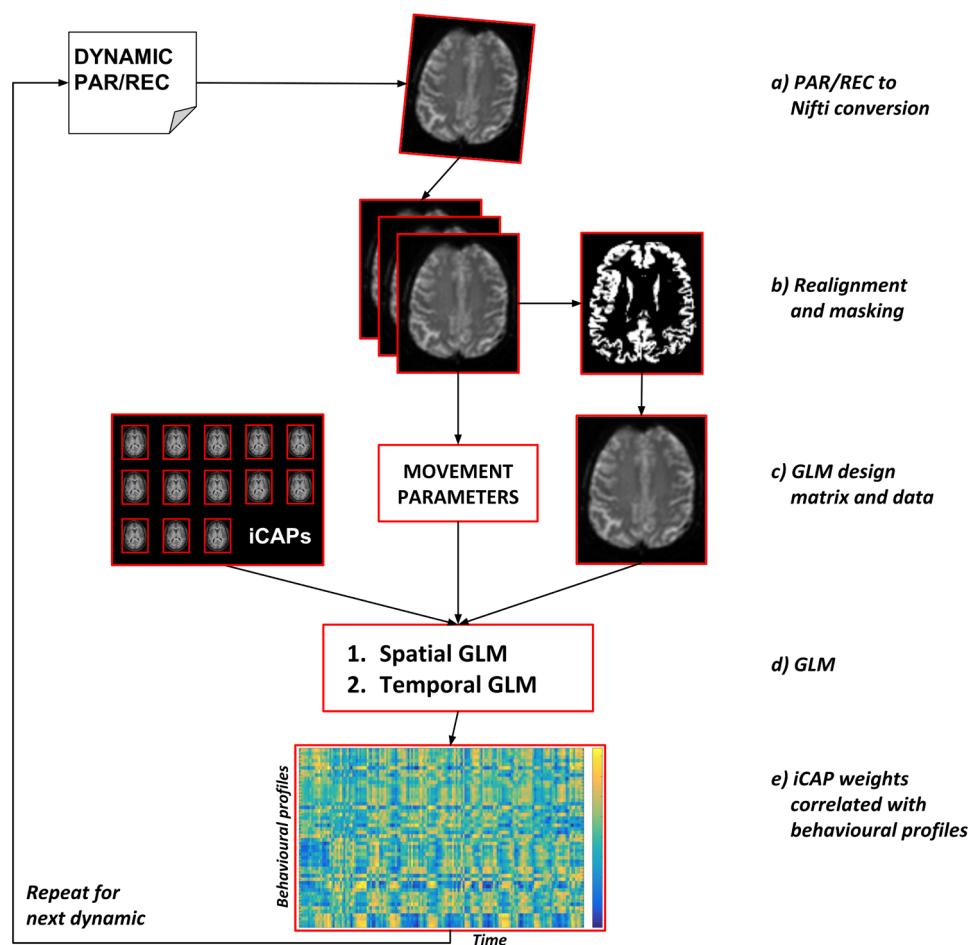
Fig. 3. The real-time processing pipeline.

profiles from the BrainMap database that fall into 5 behavioural categories: Action, Cognition, Emotion, Introception and Perception. These profiles can then be used as a means to interpret the real-time brain state of the subject.

In summary, once a dynamic image has been realigned and masked, the real-time processing entails mapping the current spatial activity pattern to a set of iCAP building blocks, yielding a set of beta weights that are subsequently detrended and then correlated with the 50 BrainMap behavioural profiles. This translates spatial patterns into possible brain states experienced by the subject in the scanner.

2.5. Experimental task design

With a set of 13 iCAPs beta-weights and a correlated set of 50 behavioural correlation coefficients being generated for each functional dynamic image, a full functional imaging run essentially contains a time series of BrainMap-database-interpreted behavioural activity fluctuations. To demonstrate our dynamic fMRI network modelling approach, i.e. to map real-time distributed brain activity to underlying iCAP patterns and subsequently to a behavioural interpretation, experiments were done with a single healthy, right-handed, male volunteer. Conditions of known block task paradigms were chosen such that the calculated behavioural activity time series could be compared with the variation in brain state expected to be induced by the stimulus or task. Controlled task paradigms included visual stimulus (watching movie clips of underwater sea life), auditory stimulus (listening to Bach) and motor task execution (finger tapping), each with a box-car design. In addition, auditory data from SPM's so-called Mother of All Experiments

(MoAE, released as part of the SPM user manual) were also analysed off-line. Experimental task paradigms for both the visual stimulus and motor task were: 16 interleaved rest and task periods of 30 s each (starting with rest), totalling an experiment run-time of 8 min. The paradigm for the auditory stimulus experiment was: 5 task periods of 60 s each, interleaved with rest periods of 30 s each (starting with rest), totalling an experiment run-time of 8 min. For the MoAE auditory data, the paradigm was: 14 interleaved rest and task periods of 42 s each (7 periods each, starting with rest), totalling an experiment run-time of 9 min 48 s.

2.6. Results Analysis

For each experiment, the behavioural time series resulting from $Neu^3CA\text{-}RT$ processing was correlated with the expected (haemodynamic response function - HRF - convolved) task time course to generate a set of Pearson's linear correlation coefficients (R) and corresponding p-values. Bonferroni correction was applied for multiple comparisons (i.e. 50 behavioural profiles); consequently, correlations with a corrected p-value below 0.001 were deemed significant. Correlations with a corrected p-value above 0.001 and below 0.002 (i.e. 0.1/50) were regarded as displaying a trend towards significance.

To investigate how well the iCAPs model described the real-time fMRI data fluctuations, the dynamic estimation error was calculated and the sum of squared estimation errors (SSE) for each experimental run was compared to the sum of squared fMRI signal (SSS) for the run. While the SSE gives an indication of the model error that can be compared between runs (by subtracting the model fit, i.e. the matrix

product of the design matrix and the estimated beta weights, from the data and calculating the square of the residual), the SSE to SSS ratio gives an indication of how large the error is compared to the actual signal (i.e. the real-time fMRI data).

3. Results

3.1. Technical results

All pre-real-time and real-time processing functionality was combined into a Matlab graphical user interface (GUI), known as *Neu³CA-RT* (Fig. 4), a video demonstration of which can be accessed on the Neu³CA website (http://neu3ca.org/project/rtfMRINF/) and for which the basic functionality is available on Github (https://github.com/jsheunis/Neu3CA-RT). The GUI allows for the specification of relevant file locations (particularly the location where real-time images are stored), the selection of pre-real-time acquired images, controlling the MRI scanner via a START/STOP command, display of real-time acquired and processed data (functional activity, task paradigm, iCAP weights and behavioural profile correlation values), as well as offline (re)processing of real-time acquired data.

Regarding timing considerations, the calculation time was logged in real-time for all processing steps of each dynamic. This included real-time file format conversion (~ 0.4 s), image realignment (~ 0.55 s), spatial GLM calculations (~ 0.08 s), temporal GLM calculations ($\sim 2.7 \times 10 - 4$ s) and correlations and visualisations (~ 0.2 s), totalling ~ 1.5 s on average. These averaged values were calculated for the three experiments with TR = 3 s described below. For the MoAE-SPM data, which had a considerably lower in-plane resolution with a 64×64 matrix size, the image realignment duration was ~ 0.3 s and the total real-time latency amounted to less than 1 s on average.

3.2. Throughput and latency

After image acquisition and pre-real-time processing steps, the current throughput of *Neu³CA-RT* amounts to 1 analysed fMRI image per TR (3 s). Pre-real-time steps include, as described, anatomical and functional image acquisition, coregistration, segmentation, mapping of the iCAPs framework to the functional space and reslicing all relevant images to the functional space resolution. During a single real-time dynamic, the throughput includes file format conversion, functional image realignment, masking, spatial and temporal GLM calculations, correlation calculations and visualisations. In *Neu³CA-RT*'s current experimental setup, the actual time required for initial image acquisition and pre-real-time processing is about 6 min and 10 min respectively. These are indicated together with the real-time latency in Fig. 5.

3.3. Experimental results

Experimental results are shown in Fig. 6 for all four experiments (*auditory, visual, motor and auditory-MoAE*), with the 50 BrainMap behavioural profiles located on the vertical axes and Pearson's linear correlation coefficient defining the unit for the horizontal axes. The correlation results are colour coded according to their corresponding corrected *p*-values, where blue shows insignificant correlation ($p > 0.002$), cyan shows a trend towards significance ($0.001 \leq p \leq 0.002$) and green indicates significant correlation ($p < 0.001$).

For improved interpretation, the top 4 positively correlated behavioural profiles from each experiment are displayed in Table 1 below, together with their *R*- and corrected *p*-values. The profiles are colour coded as explained in the caption of Fig. 6.

Additionally, to investigate how well the iCAPs model described the real-time fMRI data, the sum of squared estimation errors for each experimental run was compared to the sum of squared fMRI signal for the
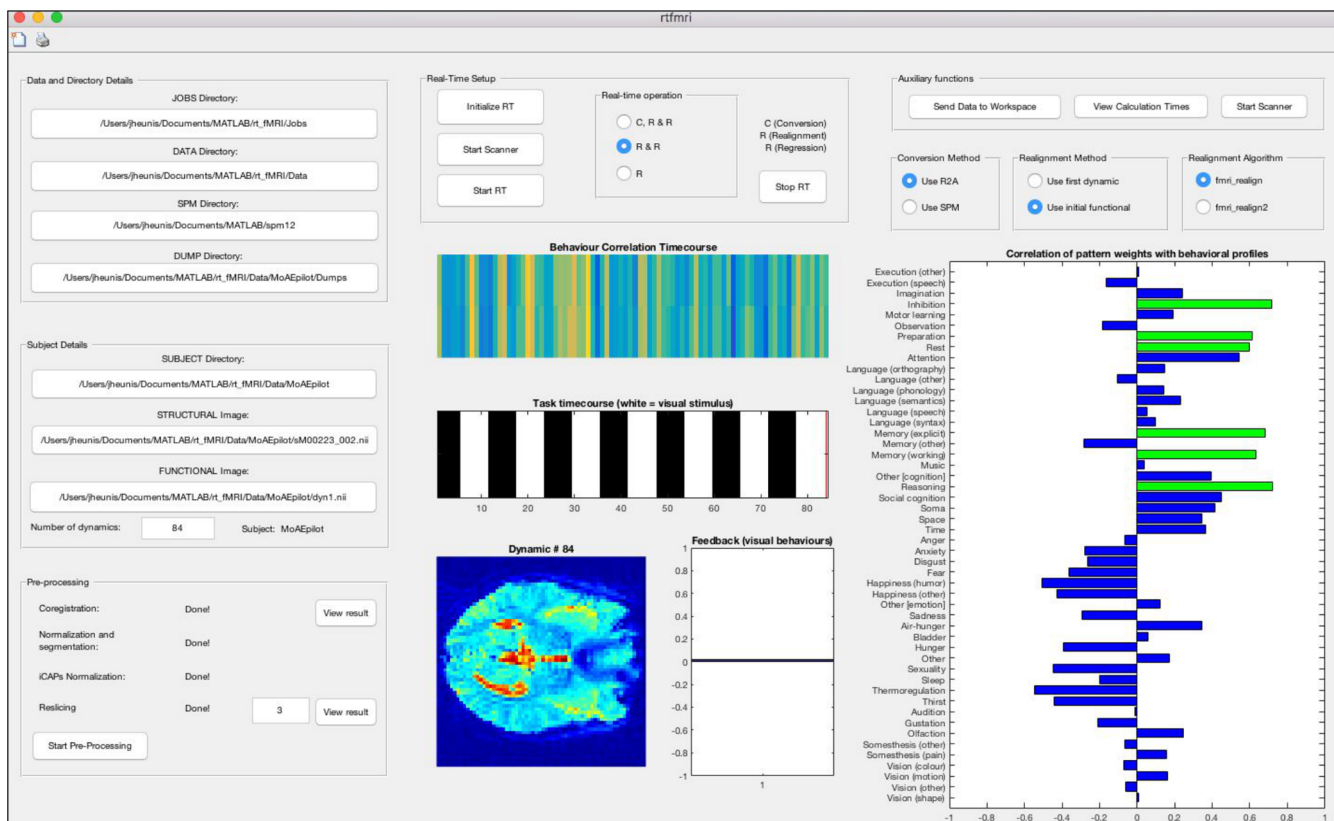

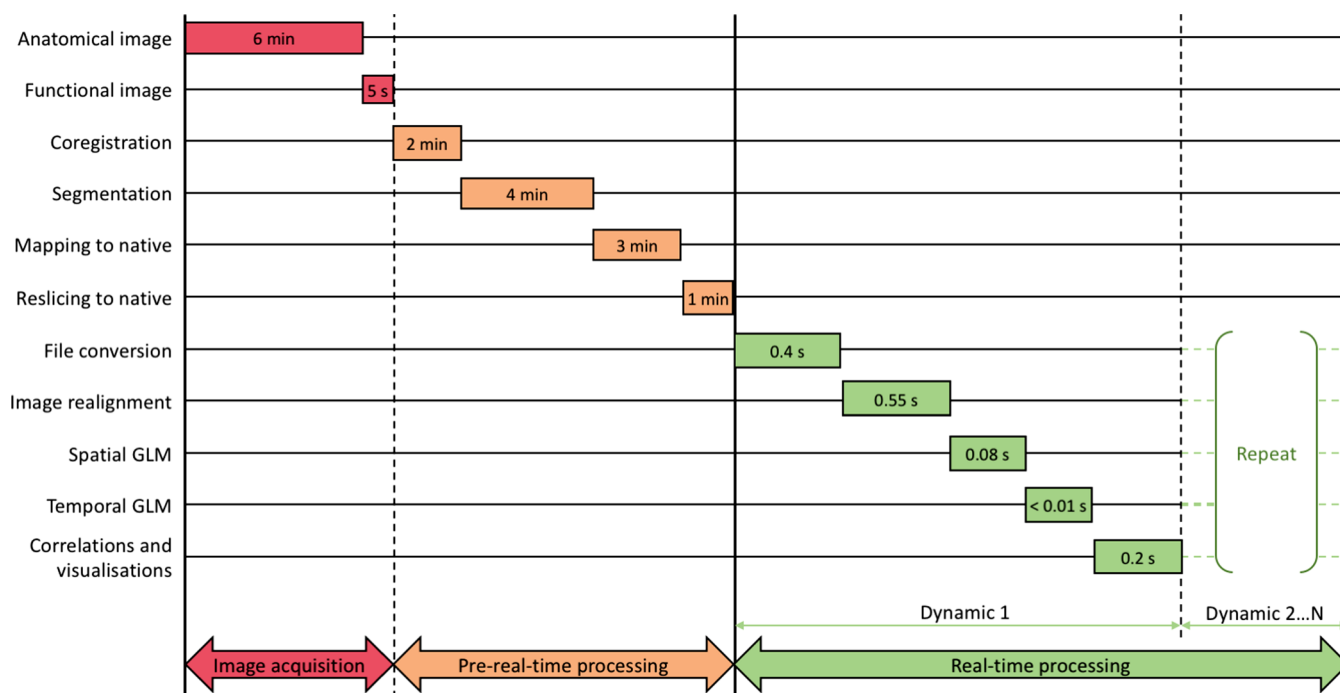**Fig. 4.** A screenshot of the *Neu³CA-RT* GUI

Fig. 5. *Neu³CA-RT's* real-time latency**. Real-time latency (green, totalling less than 2 s) is indicated on a scale with all processing steps (vertical axis). The time scale has been selectively adapted for ease of reading. (For interpretation of the references to colour in this figure legend, the reader is referred to the web version of this article.)

run. The results are shown in Fig. 7, which indicates the median (red line), 25th percentile (lower bound of blue box), 75th percentile (upper bound of blue box), upper and lower adjacent values (upper and lower black lines) and outlier values (red markers) for each of the four experimental runs. In all four cases, the sum of squared error to sum of squared signal ratio is between 0.9:1 and 1:1.

4. Discussion

4.1. Technical aspects

The importance of minimising rtfMRI calculation times has been stressed. Regarding *Neu³CA-RT's* latency performance, averages of real-time processing step calculation times indicated that image realignment had the longest duration: about 0.55 s of the available 3 s (i.e. 1 TR). In contrast, the data analysis and visualisation steps total about 0.28 s, although it must be added that the current visualisation options of *Neu³CA-RT* are not complex or resource-intensive. Considering the likely future increase of real-time processing steps (e.g. additional denoising steps and analysis algorithms, e.g. functional connectivity or MVPA methods) while keeping the throughput constant, steps should be taken to optimise for speed. It should be noted that the incorporated SPM realignment routine has several parameters (including estimation quality, interpolation techniques and reslicing options) that can be optimised for calculation speed, however the tradeoff in data quality will have to be investigated.

The real-time latency could be decreased further if no processing time is required for conversion of PAR/REC files to NIfTI by the external PC, i.e. if the vendor-supplied software exported functional images already converted to the standard NIfTI or DICOM format. However, if this conversion is handled by the vendor (either as part of the online reconstruction process or by peripheral software responsible for transporting the data) it should necessarily have a shorter execution time than the current conversion latency.

Another option worth investigating towards decreasing latency is the functional masking. Calculation time increases with the number of

voxels being processed, which could be of concern given that we focus on whole-brain analysis (as opposed to ROIs with limited voxels, assuming comparable spatial resolution) and given that increased spatial resolution could lead to improved spatial localisation. For our own experiments, the grey matter voxels of interest amounted to about 100k out of a possible 740k. Different masking methods should be investigated to minimise this number while maintaining enough multivariate data for accurate network analysis. Similarly, lower in-plane matrix sizes could be considered (as evidenced by the lower latency for the SPM-MoAE data vs the experimental data) if high spatial resolution is not particularly important for the specific analysis.

Considering overall experiment duration, Fig. 5 and the *Data Acquisition* section indicated that the typical experiment lasted about 25 min, with the initial image acquisition time being 7 min (taking time between scans into account), the pre-real-time processing time being 10 min, and the real-time latency being ~1.5 s per dynamic and 8 min in total. This is within the clinically acceptable total scan duration of 30 min to 1 h. Even so, processing steps will need to be addressed for improved data quality (the specifics of which are described below). More denoising steps or denoising steps with increased efficiency could lead to a latency increase, which should be restricted as far as possible. Apart from the options discussed above, more promising additional timesavers would be to optimise the program structure, algorithm selection and processing equipment for decreased latency of all processing steps. In this regard, apart from optimising Matlab code for speed by incorporating accepted best practices, no further in-depth consideration was given to improving program execution in the current implementation of *Neu³CA-RT*. Future work should also investigate the use of graphical processing units (GPUs), parallel computing architectures or multiplatform shared memory multiprocessing programming APIs towards decreasing real-time latency.

Finally, concerning the software infrastructure, as displayed in Fig. 1 and described previously, vendor specific software is necessary (on the scanner itself and on the external processing PC) for real-time transfer of functional images. However, *Neu³CA-RT* was created with the requirement of a server-client infrastructure, allowing future
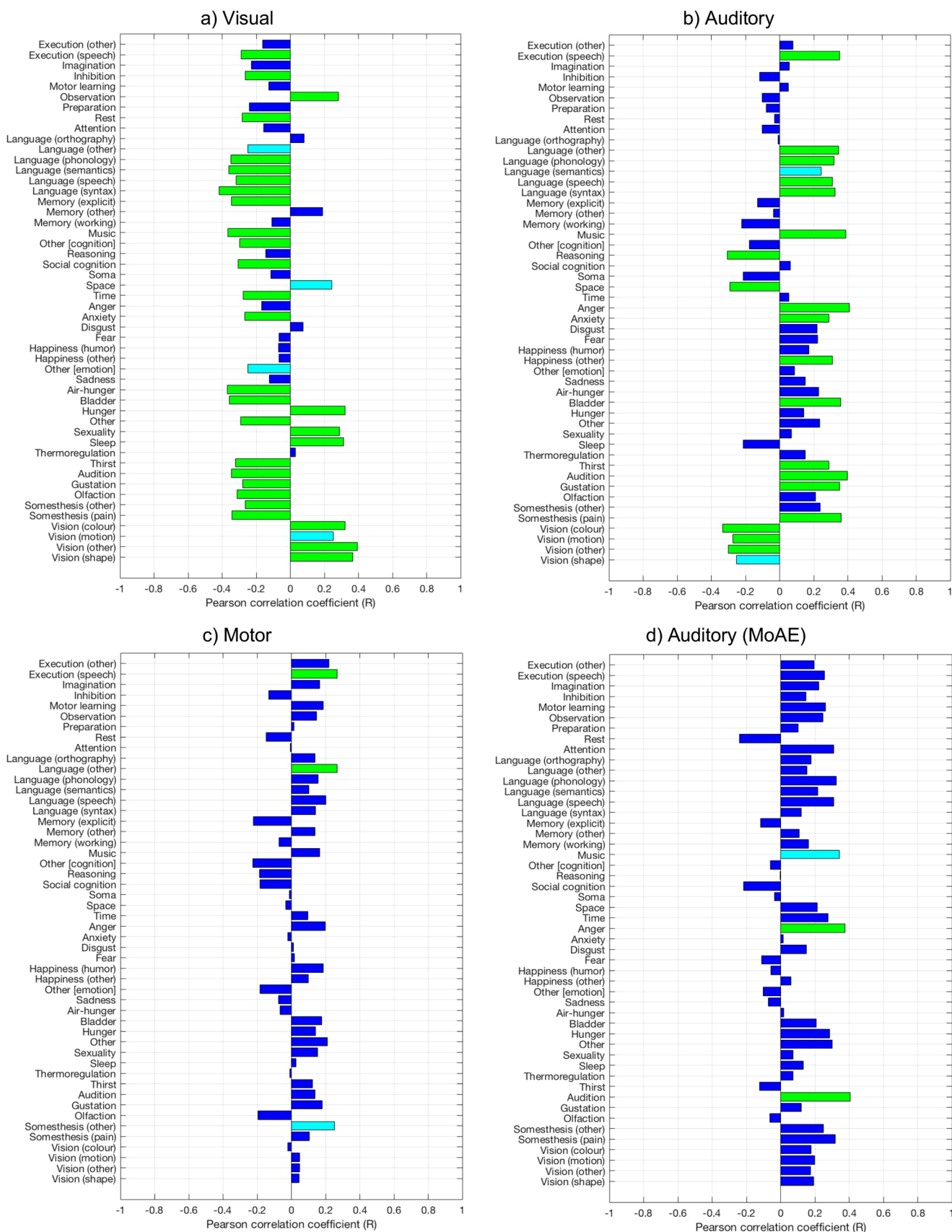
Fig. 6. Correlation results (colour-coded for *p*-values) for behavioural time series datasets (resulting from real-time processing) for different experimental task paradigms. (a) Visual stimulus, (b) Auditory stimulus, (c) Motor task execution and (d) Auditory stimulus (SPM's "Mother of All Experiments"). Colour code: Blue = insignificant correlation (*p* > 0.002), Cyan = significant trend (0.001 ≤ *p* ≤ 0.002), Green = significant correlation (*p* < 0.001). (For interpretation of the references to colour in this figure legend, the reader is referred to the web version of this article.)

Table 1
Top 4 positive correlations between HRF-convolved task time course and behavioural
profiles for multiple task paradigms

Task Paradigm	Behavioural profile	*R*-value	*p*-value
Visual stimulus	1. Vision (other)	0.3927	0.0028×10^{-4}
	2. Vision (shape)	0.3669	0.0183×10^{-4}
	3. Hunger	0.3215	0.3384×10^{-4}
	4. Vision (colour)	0.3212	0.3485×10^{-4}
Auditory stimulus	1. Anger	0.4103	0.0071×10^{-5}
	2. Audition	0.3977	0.0192×10^{-5}
	3. Music	0.3876	0.0410×10^{-5}
	4. Somesthesis (pain)	0.3618	0.2583×10^{-5}
Motor task execution	1. Execution (speech)	0.2690	0.0006
	2. Language (other)	0.2677	0.0006
	3. Somesthesis (other)	0.2530	0.0012
	4. Execution (other)	0.2202	0.0051
Auditory stimulus (MoAE-SPM)	1. Audition	0.4056	0.0001
	2. Anger	0.3757	0.0004
	3. Music	0.3415	0.0015
	4. Language (phonology)	0.3236	0.0027

integration with scanners from vendors other than Philips. In the case that scanners from other vendors output data in a proprietary file format (i.e. not NIfTI), conversion plugins will be necessary to serve data in a compatible format.

4.2. Data quality

The model estimation error investigation showed a significant difference between the actual rtfMRI data and the data described by the iCAPs model: in the order of 90%–100%, which means the error and the signal are almost equal in size. This is an undesirable outcome for a model attempting to describe as large a percentage as possible of the measured signal fluctuations. Several factors could influence this error, including: insufficient noise regressors or confounding regressors in the spatial GLM (for example, real-time physiological data were unavailable and thus not corrected for in the current Neu^3CA-RT implementation); not accounting for other possible artefacts like EPI signal dropout or scanner induced distortion; processing fMRI data at suboptimal BOLD contrast; and incorrect model definition. If it can be established that said artefacts have significant detrimental effects on the quality of these experimental rtfMRI data, they should first be

corrected for before further analysis iterations can shed light on the remaining error and the resulting performance of the iCAPs model. Thus, although realignment residuals and signal drift were already corrected for in the current implementation, improved noise modelling and removal techniques should be investigated. Because masks were calculated in the functional space for grey matter, white matter and CSF, the latter two could be used to generate averaged noise compartment signals to be used as extra regressors in the denoising GLM.

Whether improved preprocessing steps result in an improved fit of the iCAPs model to the experimental data or not, or if completely different models or analysis techniques are applied in future, accurate preprocessing for improved data quality remains of utmost importance.

4.3. Network-based analysis

In the real-time fMRI analysis method explored in this work, a brain-wide multi-voxel approach was used to characterise modulation of distributed brain activity during a known task paradigm as a set of innovation-driven co-activation pattern fluctuations, which were interpretable as correlated behavioural profile fluctuations. The main aim was to develop a toolbox that allows the analysis of whole-brain
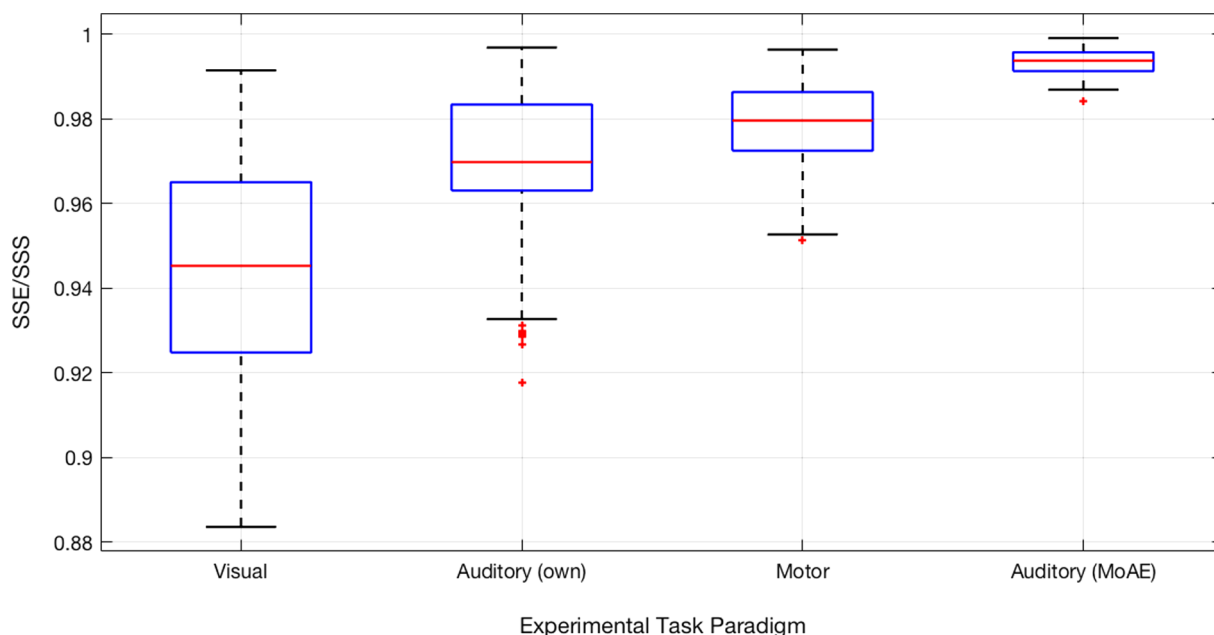
Fig. 7. Sum of squared errors (SSE) divided by sum of squared signal (SSS). SSE/SSS (on the vertical axis, lowest value at 0.88 for easier comparability) is shown for each of the four experimental runs (on the horizontal axis).

networks as the basis for eventually calculating a neurofeedback signal, as networks are hypothesized to contain richer information about the underlying condition being studied (as compared to ROI-based analysis). Measures of brain network fluctuation and interaction could thus serve as contingent neurofeedback signals with the aim of increasing training effects in rtfMRI neurofeedback studies.

Our proof-of-concept network-based analysis consisted of fitting a model of temporally and spatially overlapping co-activation patterns, regarded as building-blocks of standard resting state networks (Karahanoğlu and Van de Ville, 2015), to real-time denoised fMRI data using a spatial GLM. For each timepoint in a functional time series, the beta weights resulting from the GLM were transformed to correlation values with 50 behavioural profiles from the BrainMap database, essentially yielding a real-time behavioural interpretation of the subject's brain state. These behavioural time series were then correlated with their respective experimental task designs to find specific behavioural profiles that correlated with the task or stimulus time series. This was compared against expected behaviours given the task or stimulus.

The results indicated expected effects in three out of the four experiments, where the most significant positive correlation between a BrainMap behavioural profile time course and the experimental task design was shown for an expected brain state. Table 1 summarised this result: for a visual stimulus, *Vision* had the most significant correlation; for an auditory stimulus (MoAE-SPM data), *Audition*; and for a motor task, *Execution (speech)*. It should be noted that the *Execution (speech)* profile might detract from the results' accuracy, as *Execution (other)* seems like a more logical expectation, although it is known that speech involves complex articular movement and that the sensorimotor and language networks involve common anatomy (Besseling et al., 2013). Unexpected results in the top 4 positively correlated behavioural profiles are also noted for each experiment: for the visual experiment, *Hunger* is unexpected; and for both auditory experiments, *Anger* is unexpected. This occurrence of unexpected effects was not limited to within-behavioural-category profiles, as is demonstrated by the *Hunger* profile (from the category, *Introception*) being significantly correlated with the visual experiment task design. The fact that more significant effects (and trends towards such effects) were found than were expected indicates a lack of specificity of the analysis method. Furthermore, the observed correlation values in all experiments were relatively low,

reaching a maximum of 0.4103 for behavioural profile *Anger* in the auditory stimulus experiments.

For the experiments under consideration, the investigation was limited to task-positive correlations in a single subject in an attempt to identify significant up-regulated behaviour for a given task paradigm. This design decision, however, posited no claims as to the importance of significant and simultaneous task-negative correlations, nor to simultaneous but unexpected up-regulations, nor to the relative correlation values. An example of strong negative correlation between behavioural profiles and the task design was found in all language profiles for both the visual and auditory experiment. Further investigation, with an increase in statistical power, is required into the dynamics of simultaneous and opposing behavioural profile fluctuations to shed light on this observation, specifically given the known spatially distributed and dynamic nature of human brain networks.

Furthermore, the iCAPs and BrainMap behavioural profile model used in this study was selected as an exploratory method based on their hypothesized usefulness as targets for neurofeedback in neuropsychiatric conditions, given the spatially distributed and dynamic nature of the patterns and the intuitive relation to brain state interpretations. This, however, does not preclude the use of other network-based analysis methods in *Neu³CA-RT*. With some updates to the code, it is possible to use the framework with different network models hypothesized to underlie whichever whole-brain mechanism is being studied and used for neurofeedback training.

4.4. Future work

Although the current implementation of *Neu³CA-RT* serves as a successful proof of concept of a network analysis driven rtfMRI framework, the discussion items indicate that further development and testing is required, especially with regards to improving technical implementation, network analysis and data quality.

Regarding *Neu³CA-RT*'s technical implementation and software design, aside from adding improved artefact monitoring and visualisation options to the toolbox, particular attention will be given to: minimising the latency of each step in the real-time processing pipeline; minimising the latency added by the Matlab GUI infrastructure (either by using a compiled version of Matlab or a different programming framework);

investigating increased processing power and parallelization options; and updating the GUI for intuitive user experience.

To improve the network analysis presented in this study, the first aim should be to use a better understanding of the behavioural profile dynamics to propose an efficient model that increases the specificity of the results, an aspect that the *Neu³CA-RT* framework currently lacks. With increased specificity, more complete and intuitive interpretations can be made from the results about the dynamic brain state of the subject and hence about the validity of the iCAPs/BrainMap network analysis model in a rtfMRI framework. In future, network analysis need not be limited to the iCAPs model and should be expanded to include other network models as well as MVPA, data-driven and/or machine learning methods known in literature to yield improved results.

Envisaged steps to investigate and improve data quality include: adding real-time white matter and CSF nuisance regressors to the denoising GLM; correcting for physiological noise in real-time (heart beat and breathing); correcting for scanner induced artefacts in real-time; improving software options to display subject movement and other noise in real-time (i.e. quality checking); and optimising BOLD contrast and sensitivity with the use of real-time multi-echo EPI acquisition and processing.

Finally, while this work reported the development and explorative use of a real-time fMRI analysis tool based on whole-brain networks, the ultimate goal of *Neu³CA-RT* is for it to be used as a tool in rtfMRI neurofeedback training experiments. In this regard, several data processing steps should be added to the real-time pipeline, including neurofeedback signal calculation, scaling and presentation. Once future developments with regards to rtfMRI data denoising and quality improvements have been accomplished, a neurofeedback experiment could investigate the effects of neurofeedback-driven modulation of one or a set of the behavioural profiles, as these profiles provide a simple representation of complex network-based and dynamic brain activity.

Acknowledgements

Conflict of interest

RL and MB are, respectively, employees of Philips Research and Philips Healthcare in The Netherlands. The other authors have declared that no further competing interests exist.

Contributors

Conceived and designed the experiments: S.H. R.B. R.L. A.d.L.. Performed the experiments: S.H. R.B. R.L. Analyzed the data: S.H. R.B. Contributed reagents/materials/analysis tools: S.H. R.B. R.L. Wrote the paper: SH. Reviewed the paper: R.B. R.L. A.d.L. M.B. B.A. J.B.

Supplementary materials

Supplementary material associated with this article can be found, in the online version, at doi:10.1016/j.pscychresns.2018.09.008.

References

Alegria, A.A., Wulff, M., Brinson, H., Barker, G.J., Norman, L.J., Brandeis, D., et al., 2017. Real-time fMRI neurofeedback in adolescents with attention deficit hyperactivity disorder. Hum. Brain Mapp. https://doi.org/10.1002/hbm.23584.

Bagarinao, E., Matsuo, K., Nakai, T., Sato, S., 2003. Estimation of general linear model coefficients for real-time application. NeuroImage. https://doi.org/10.1016/S1053-8119(03)00081-8.

Bandettini, P., Wong, E., Hinks, R., Tikofsky, R., Hyde, J., 1992. Time course EPI of human brain function during task activation. Magn. Reson. Med. https://doi.org/10.1002/mrm.1910250220.

Beckmann, C., Deluca, M., Devlin, J., Smith, S., 2005. Investigations into resting-state connectivity using independent component analysis. Philos. Trans. R. Soc. Lond. B Biol. Sci. https://doi.org/10.1098/rstb.2005.1634.

Besseling, R., Jansen, J., Overvliet, G., Van Der Kruijs, S., Vles, J., Ebus, S., et al., 2013. Reduced functional integration of the sensorimotor and language network in rolandic epilepsy. NeuroImage Clin. https://doi.org/10.1016/j.nicl.2013.01.004.

Binder, J.R., 2011. Functional MRI is a valid noninvasive alternative to Wada testing. Epilepsy Behav. https://doi.org/10.1016/j.yebeh.2010.08.004.

Caria, A., Sitaram, R., Birbaumer, N., 2012. Real-time fMRI. Neuroscientist. https://doi.org/10.1177/1073858411407205.

Cohen, M.S., 2001. Real-time functional magnetic resonance imaging. Methods 25 (2), 201–220. https://doi.org/10.1006/meth.2001.1235.

Collins, D., Neelin, P., Peters, T., Evans, A., 1994. Automatic 3D intersubject registration of MR volumetric data in standardized Talairach space. J. Comput. Assist. Tomo. https://doi.org/10.1097/00004728-199403000-00005.

Cox, R.W., Jesmanowicz, A., Hyde, J.S., 1995. Real-time functional magnetic resonance imaging. Magn. Reson. Med 33 (2), 230–236. https://doi.org/10.1002/mrm.1910330213.

Cox, R.W., 1996. AFNI: software for analysis and visualization of functional magnetic resonance neuroimages. Comput. Biomed. Res. https://doi.org/S0010480996900142.

deCharms, R.C., 2007. Reading and controlling human brain activation using real-time functional magnetic resonance imaging. Trends Cogn. Sci 11 (11), 473–481. https://doi.org/10.1016/j.tics.2007.08.014.

deCharms, R.C., 2008. Applications of real-time fMRI. Nat. Rev. Neurosci. https://doi.org/10.1038/nrn2414.

Esposito, F., Seifritz, E., Formisano, E., Morrone, R., Scarabino, T., Tedeschi, G., et al., 2003. Real-time independent component analysis of fMRI time-series. NeuroImage. https://doi.org/10.1016/j.neuroimage.2003.08.012.

Gao, K., Posse, S., 2003. TurboFIRE: Real-time fMRI with automated spatial normalization and Talairach Daemon database. In: Abstract at 9th Annual Meeting of the OHBM. New York, USA.

Gembris, D., Taylor, J.G., Schor, S., Frings, W., Suter, D., Posse, S., 2000. Functional magnetic resonance imaging in real time (FIRE): Sliding- window correlation analysis and reference-vector optimization. Magn. Reson. Med. https://doi.org/10.1002/(SICI)1522-2594(200002)43:2<259::AID-MRM13>3.0.CO;2-P.

Goebel, R., 2012. BrainVoyager - past, present, future. NeuroImage. https://doi.org/10.1016/j.neuroimage.2012.01.083.

Hellrung, L., Hollmann, M., Zscheyge, O., Schlumm, T., Kalberlah, C., Roggenhofer, E., et al., 2015. Flexible adaptive paradigms for fMRI using a novel software package 'brain analysis in real-time ' (BART). PLoS One. https://doi.org/10.1371/journal.pone.0118890.

Hirsch, J., Ruge, M.I., Kim, K.H.S., Correa, D.D., Victor, J.D., Relkin, N.R., et al., 2000. An integrated functional magnetic resonance imaging procedure for preoperative mapping of cortical areas associated with tactile, motor, language, and visual functions. Neurosurgery. https://doi.org/10.1227/00006123-200009000-00037.

Karahanoğlu, F.I., Van De Ville, D., 2015. Transient brain activity disentangles fMRI resting-state dynamics in terms of spatially and temporally overlapping networks. Nat. Commun. https://doi.org/10.1038/ncomms8751.

Koush, Y., Rosa, M.J., Robineau, F., Heinen, K., W. Rieger, S., Weiskopf, N., Vuilleumier, P., Van De Ville, D., Scharnowski, F., 2013. Connectivity-based neurofeedback: Dynamic causal modeling for real-time fMRI. NeuroImage 81, 422–430. https://doi.org/10.1016/j.neuroimage.2013.05.010.

Koush, Y., Ashburner, J., Prilepin, E., Sladky, R., Zeidman, P., Bibikov, S., et al., 2017. OpenNFT: An open-source Python/Matlab framework for real-time fMRI neurofeedback training based on activity, connectivity and multivariate pattern analysis. Neuroimage. https://doi.org/10.1016/j.neuroimage.2017.06.039.

Kundu, P., Inati, S., Evans, J., Luh, W., Bandettini, P., 2012. Differentiating BOLD and non-BOLD signals in fMRI time series using multi-echo EPI. NeuroImage. https://doi.org/10.1016/j.neuroimage.2011.12.028.

Kundu, P., Brenowitz, N., Voon, V., Worbe, Y., Vértes, P., Inati, S., et al., 2013. Integrated strategy for improving functional connectivity mapping using multiecho fMRI. In: Proceedings of the National Academy of Sciences of the Unites States of America, . https://doi.org/10.1073/pnas.1301725110.

Kundu, P., Voon, V., Balchandani, P., Lombardo, M., Poser, B., Bandettini, P., 2017. Multi-echo fMRI: A review of applications in fMRI denoising and analysis of BOLD signals. NeuroImage. https://doi.org/10.1016/j.neuroimage.2017.03.033.

LaConte, S.M., Peltier, S.J., Hu, X.P., 2007. Real-time fMRI using brain-state classification. Hum. Brain Mapp 28, 1033–1044. https://doi.org/10.1002/hbm.20326.

LaConte, S.M., 2011. Decoding fMRI brain states in real-time. Neuroimage. https://doi.org/10.1016/j.neuroimage.2010.06.052.

Laird, A., Lancaster, J., Fox, P., 2005. BrainMap: The social evolution of a human brain mapping database. Neuroinformatics. https://doi.org/10.1385/NI:3:1:065.

Lui, S., Zhou, X.J., Sweeney, J.A., Gong, Q., 2016. Psychoradiology: The frontier of neuroimaging in psychiatry. Radiology. https://doi.org/10.1148/radiol.2016152149.

Magland, J.F., Tjoa, C.W., Childress, A.R., 2011. Spatio-temporal activity in real time (STAR): Optimization of regional fMRI feedback. Neuroimage. https://doi.org/10.1016/j.neuroimage.2010.12.085.

Mišić, B., Sporns, O., 2016. From regions to connections and networks: new bridges between brain and behavior. Curr. Opin. Neurobiol. 40, 1–7. https://doi.org/10.1016/j.conb.2016.05.003.

Nicholson, A.A., Rabellino, D., Densmore, M., Frewen, P.A., Paret, C., Kluetsch, R., et al., 2017. The neurobiology of emotion regulation in posttraumatic stress disorder:

Amygdala downregulation via real-time fMRI neurofeedback. Hum. Brain Mapp. https://doi.org/10.1002/hbm.23402.

Oostenveld, R., Fries, P., Maris, E., Schoffelen, J.M., 2011. FieldTrip: Open source software for advanced analysis of MEG, EEG, and invasive electrophysiological data. Comput. Intell. Neurosci 2011, 156869. https://doi.org/10.1155/2011/156869.

Posse, S., Wiese, S., Gembris, D., Mathiak, K., Kessler, C., Grosse-Ruyken, M., et al., 1999. Enhancement of BOLD-contrast sensitivity by single-shot multi-echo functional MR imaging. Magn. Reson. Med. 42, 87–97. https://doi.org/10.1002/(SICI)1522-2594(199907)42:1 < 87::AID-MRM13 > 3.0.CO;2-O.

Ruiz, S., Birbaumer, N., Sitaram, R., 2013. Abnormal neural connectivity in schizophrenia and fMRI-brain-computer interface as a potential therapeutic approach. Front. Psychiatry. https://doi.org/10.3389/fpsyt.2013.00017.

Sato, J.R., Basilio, R., Paiva, F.F., Garrido, G.J., Bramati, I.E., Bado, P., et al., 2013. Real-time fMRI pattern decoding and neurofeedback using FRIEND: An FSL-integrated BCI toolbox. PLoS One. https://doi.org/10.1371/journal.pone.0081658.

Sitaram, R., Ros, T., Stoeckel, L., Haller, S., Scharnowski, F., Lewis-Peacock, J., et al., 2016. Closed-loop brain training: The science of neurofeedback. Nat. Rev. Neurosci. https://doi.org/10.1038/nrn.2016.164.

Smink, J., Häkkinen, M., Holthuizen, S., Krueger, S., Ries, M., Berber, Y., et al., 2011. eXTernal Control (XTC): A flexible, real-time, low-latency, bi-directional scanner interface. In: Proceedings of the International Society for Magnetic Resonance in Medicine, pp. 19.

Smyser, C., Grabowski, T., Frank, R., Haller, J., Bolinger, L., 2001. Real-time multiple linear regression for fMRI supported by time-aware acquisition and processing. Magn. Reson. Med. https://doi.org/10.1002/1522-2594(200102)45:2 < 289::AID-MRM1038 > 3.0.CO;2-U.

Subramanian, L., Hindle, J.V., Johnston, S., Roberts, M.V., Husain, M., Goebel, R., et al., 2011. Real-time functional magnetic resonance imaging neurofeedback for treatment of Parkinson's disease. J. Neurosci. https://doi.org/10.1523/JNEUROSCI.3498-11.2011.

Sulzer, J., Haller, S., Scharnowski, F., Weiskopf, N., Birbaumer, N., Blefari, M.L., et al., 2013. Real-time fMRI neurofeedback: Progress and challenges. NeuroImage. https://doi.org/10.1016/j.neuroimage.2013.03.033.

Weiskopf, N., Scharnowski, F., Veit, R., Goebel, R., Birbaumer, N., Mathiak, K., 2004. Self-regulation of local brain activity using real-time functional magnetic resonance imaging (fMRI). J. Physiol. Paris Decod. Interfac. Brain 98, 357–373. https://doi.org/10.1016/j.jphysparis.2005.09.019.

Weiskopf, N., Klose, U., Birbaumer, N., Mathiak, K., 2005. Single-shot compensation of image distortions and BOLD contrast optimization using multi-echo EPI for real-time fMRI. Neuroimage 2005. https://doi.org/10.1016/j.neuroimage.2004.10.012.

Weiskopf, N., Sitaram, R., Josephs, O., Veit, R., Scharnowsk, F., Goebel, R., et al., 2007. Real-time functional magnetic resonance imaging: Methods and applications. Magn. Reson. Imaging. 25 (6), 989–1003. https://doi.org/10.1016/j.mri.2007.02.007.

Weiskopf, N., 2012. Real-time fMRI and its application to neurofeedback. NeuroImage. https://doi.org/10.1016/j.neuroimage.2011.10.009.

Whitfield-Gabrieli, S., Ford, J.M., 2012. Default mode network activity and connectivity in psychopathology. Annu. Rev. Clin. Psychol. 8, 49–76. https://doi.org/10.1146/annurev-clinpsy-032511-143049.

Voyvodic, J.T., 1999. Real-time fMRI paradigm control, physiology, and behavior combined with near real-time statistical analysis. Neuroimage. https://doi.org/10.1006/nimg.1999.0457.

Young, K., Siegle, G., Zotev, V., Phillips, R., Misaki, M., Yuan, H., et al., 2017. Randomized clinical trial of real-time fMRI Amygdala Neurofeedback for major depressive disorder: Effects on symptoms and autobiographical memory recall. Am. J. Psychiatry. https://doi.org/10.1176/appi.ajp.2017.16060637.

Zaitsev, M., Dold, C., Sakas, G., Hennig, J., Speck, O., 2006. Magnetic resonance imaging of freely moving objects: Prospective real-time motion correction using an external optical motion tracking system. NeuroImage 2006. https://doi.org/10.1016/j.neuroimage.2006.01.039.

Zilverstand, A., Sorger, B., Zimmermann, J., Kaas, A., Goebel, R., 2014. Windowed correlation: A suitable tool for providing dynamic fMRI-based functional connectivity neurofeedback on task difficulty. Plos One. 9. https://doi.org/10.1371/journal.pone.0085929.